Chiral self-assembly of enantiomerically pure (4S,7R)-campho[2,3-c]pyrazole in the solid state: A vibrational circular dichroism (VCD) and computational study

ARTICLE *in* TETRAHEDRON ASYMMETRY · APRIL 2014

Impact Factor: 2.16 · DOI: 10.1016/j.tetasy.2014.02.015

7 AUTHORS, INCLUDING:

J. J. López González
Universidad de Jaén
134 PUBLICATIONS **1,138** CITATIONS
SEE PROFILE

Rosa M Claramunt
National Distance Education University
472 PUBLICATIONS **5,608** CITATIONS
SEE PROFILE

Concepción López
National Distance Education University
95 PUBLICATIONS **1,084** CITATIONS
SEE PROFILE

Ibon Alkorta
Spanish National Research Council
679 PUBLICATIONS **12,389** CITATIONS
SEE PROFILE

Tetrahedron: *Asymmetry* 25 (2014) 507–515

Contents lists available at ScienceDirect

Tetrahedron: *Asymmetry*

journal homepage: www.elsevier.com/locate/tetasy

Chiral self-assembly of enantiomerically pure (4*S*,7*R*)-campho[2,3-*c*]pyrazole in the solid state: a vibrational circular dichroism (VCD) and computational study

María Mar Quesada-Moreno [a], Juan Ramón Avilés-Moreno [a], Juan Jesús López-González [a,*], Rosa María Claramunt [b,*], Concepción López [b], Ibon Alkorta [c,*], José Elguero [c]

[a] *Departamento de Química Física y Analítica, Universidad de Jaén, Campus Las Lagunillas, E-23071 Jaén, Spain*
[b] *Departamento de Química Orgánica y Bio-Orgánica, Facultad de Ciencias, Universidad Nacional de Educación a Distancia (UNED), Senda del Rey 9, E-28040 Madrid, Spain*
[c] *Instituto de Química Médica (CSIC), Juan de la Cierva, 3, E-28006 Madrid, Spain*

ARTICLE INFO

Article history:
Accepted 27 February 2014

ABSTRACT

NH-Indazoles in solid phase usually form N—H···N hydrogen bonds between positions 1 and 2, which determine the secondary structure, forming dimers, trimers, or catemers (chains). Thus, the difficulty of the experimental analysis of the structure of the family of 1*H*-indazoles is clear. We have outlined a complete strategy by using different techniques of vibrational spectroscopy that are sensitive (VCD) and not sensitive (IR, FarIR, and Raman) to the chirality together with quantum chemical calculations. We have studied the chiral structure of (4*S*,7*R*)-campho[2,3-*c*]pyrazole both in solution (CCl_4) and in the solid phase (crystal). This compound crystallizes as a chiral trimer (**LABHEB**), with the monomer also being chiral. Herein, Far-IR, IR, and Raman spectra in solution and in the solid state are assigned using the support of B3LYP/6-31G(d) and B97D/6-31+G(d,p) calculations of (4*S*,7*R*)-campho[2,3-*c*]pyrazole monomers, dimers, and trimers, these last cyclamers being partially and fully optimized. Later, analysis of the vibrational circular dichroism (VCD) spectra allowed us to determine the chiral self-assembly of (4*S*,7*R*)-campho[2,3-*c*]pyrazole crystals (**LABHEB**). In the crystal, only the trimers are present while in solution, the monomer predominates. We have highlighted the importance of the analysis of the low frequency region (700–25 cm^{-1}) in the FT-Raman and Far-IR spectra, because it provides relevant information in order to confirm the presence of the trimers in the solid phase.

1. Introduction

Over the last few years, we have been interested in the crystal structure of N*H*-pyrazoles[1] and N*H*-indazoles.[2] In particular, we have studied two aspects, proton transfers (solid-state proton transfer, SSPT)[3] and chirality.[4–12] Herein we deal with the second aspect.

When one considers the structures of N*H*-indazoles reported in the Cambridge Structural Database,[13] four types of situations occur concerning the network of hydrogen bonds present in all cases. There are many examples where there are functional groups at the 3, 4, 5, 6, or 7 positions such as NHR, CONHR, CO_2H, or NO_2, that prevent or accompany the N—H···N hydrogen bonds and that will not be considered here. In those cases where the N—H···N hydrogen bonds between the 1- and 2-positions determine the secondary structure, indazoles crystallize forming dimers, trimers, or catemers (chains).[14] A second aspect that is particularly relevant herein is represented in Scheme 1.

If the monomer is chiral, then the crystal is also chiral. This is the case for the (4*S*,7*R*)-7,8,8-trimethyl-4,5,6,7-tetrahydro-4,7-methano-2*H*-indazole **LABHEB,** (**LABHEB** is the code used by the CSD to identify this compound),[13] commonly known as (4*S*,7*R*)-campho[2,3-*c*]pyrazole since it is prepared from natural camphor [(1*R*,4*R*)-(+)]. The structure has been determined twice, first by us in 1993 at 295 K[4] and in 2007 at 150 K by other authors.[15] This compound crystallizes in the $P2_1$ space group as two trimers (Scheme 1 and Fig. 1) formed by six independent molecules (average dN···N = 2.923 Å). The position of the tautomeric proton is 2 instead of 1 for all other indazoles, due to the absence of the phenyl ring that destabilized the quinonoid form.

If the monomer is achiral, the most common case is that the crystal is also achiral, with it usually being a dimer or a trimer; if it is a catemer, then both helices are present in the unit cell. An

* Corresponding authors. Tel.: +34 953212754 (J.J.L.G.); +34 913987322 (RMC); +34 912587410 (IA).
E-mail addresses: jjlopez@ujaen.es (J.J. López-González), rclaramunt@ccia.uned.es (R.M. Claramunt), ibon@iqm.csic.es (I. Alkorta).

http://dx.doi.org/10.1016/j.tetasy.2014.02.015
0957-4166/

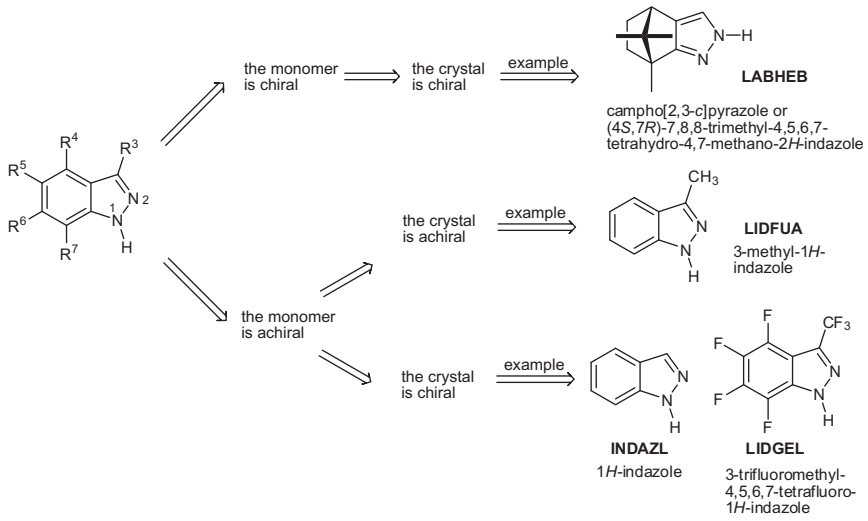

Scheme 1. The different situations present in crystals of N*H*–indazoles.[13]

example of this group is the case of 3-methyl-1*H*-indazole **LIDFUA** crystallizing as a dimer.[9]

There are some examples of 1*H*-indazoles that crystallize as catemers, where only one enantiomer is present in the unit cell for a given crystal that can be separated manually (spontaneous resolution). This is the case for 1*H*-indazole **INDAZL**,[11] and for 3-trifluoromethyl-4,5,6,7-tetrafluoro-1*H*-indazole **LIDGEL**,[9] which we have already studied by VCD.

Herein, we will examine the chiroptical properties of (4*S*,7*R*)-campho[2,3-*c*]pyrazole in relation to its structure by means of: (a) DFT calculations for simulation of the chiral trimer found in the crystal, which was partially (only hydrogen atoms) and fully optimized (the structure of the trimer has been modeled starting from the X-ray structure); (b) experimentally, as a first step, we have analyzed the IR-FarIR-Raman spectra in solution and solid phases in order to establish the presence of monomers and trimers; (c) analysis of the VCD spectra in solution and solid phases with special attention paid to the chiral self-assembly of the **LABHEB** crystals. It should be noted that although we use the code-name **LABHEB** to assign this compound, this is only true for the solid state; in solution the monomer is (4*S*,7*R*)-campho[2,3-*c*]pyrazole.

2. Results and discussion

2.1. Chiral self-assembly and the structure of LABHEB crystals

The availability of VCD experimental and theoretical data could be helpful for achieving our aim and for a better knowledge of the chiral self-assembly structure of (4*S*,7*R*)-campho[2,3-*c*]pyrazole in solution and solid phases. Our experience is that a previous vibrational analysis for them, from Far-IR, IR, and Raman data and quantum chemical calculations, is a recommended approach when possible.[16]

Thus, our method was as follows: (1) recording of Far-IR, IR, VCD, and Raman spectra of **LABHEB** in CCl_4, film and nujol/fluorolube mulls; (2) then comparing these spectra with the calculated B3LYP/6-31G(d) and B97D/6-31+G(d,p) spectra of the monomer, the dimer, and the trimer the (partially and fully optimized) after using a frequency scale factor of 0.960 and 1.020, respectively, from the NIST database.[17]

The geometry of the monomer, the dimer, and the trimers has been fully optimized at the B3LYP/6-31G(d) and B97D/6-31+G(d,p) computational levels. Furthermore, the two independent trimers found in the **LABHEB** crystal by X-ray study have been partially optimised, the geometry of the hydrogen atoms has been optimized while keeping the positions of the heavy atoms fixed to that found in the crystal structure. While in the trimer, fully optimised, the N—H···N intermolecular distances have the same value (191 pm), such lengths of both trimers slightly differ in the crystal structure. Thus in the first trimer, two intermolecular N···N of 291 pm and one of 294 pm are present, while the second trimer shows two distances of 293 pm and one of 291 pm. The structures of the aforementioned trimers have been fixed to their crystal geometry because of their importance in order to characterize the chiroptical response of the **LABHEB** crystals.

The results obtained with both functionals are similar in terms of structure and predicted IR, Raman, and VCD harmonic frequencies and intensities. For the sake of clarity, the B3LYP and B97D results are plotted in all of the figures presented below.

2.2. IR and Raman spectra

We have divided the vibrational assignment of IR and Raman spectra into a few regions (N—H stretching, C—H stretching, intermediate and low frequency regions) to explain the discussion clearly. In order to understand the vibrational spectra of **LABHEB**, we will make remarks about the most relevant spectroscopic features.

DFT calculations have been carried out in the harmonic approximation. It does not consider overtones and combination bands. Therefore, some bands of IR and Raman spectra are not predicted.

In the N—H and C—H stretching region some bands could be assigned to different normal modes, because large overlapping is seen (see Figs. 2a and b, 3a and b). The experimental band observed at 3480 cm^{-1} (IR in CCl_4 solution) is assigned to the free N—H stretching normal mode of the monomer structure. However, this band was not observed in the IR spectrum under film conditions. In both IR spectra, film and solution, the experimental bands at 3178 cm^{-1} (IR, 3174 cm^{-1} in Raman), 3148 cm^{-1}, and at 3109 cm^{-1} (IR and Raman) correspond to the three symmetric and asymmetric linked N—H stretchings and to the three vinyl hydrogen stretchings of the trimer structures. Furthermore, the experimental bands observed at 2984 cm^{-1} (IR, 2982 cm^{-1} in Raman), 2955 cm^{-1} (IR, 2958 cm^{-1} in Raman), 2919 cm^{-1} (IR and Raman), and at 2866 cm^{-1} (IR, 2863 cm^{-1} in Raman) were assigned to the C—H stretching of the CH_3 and CH_2 groups.

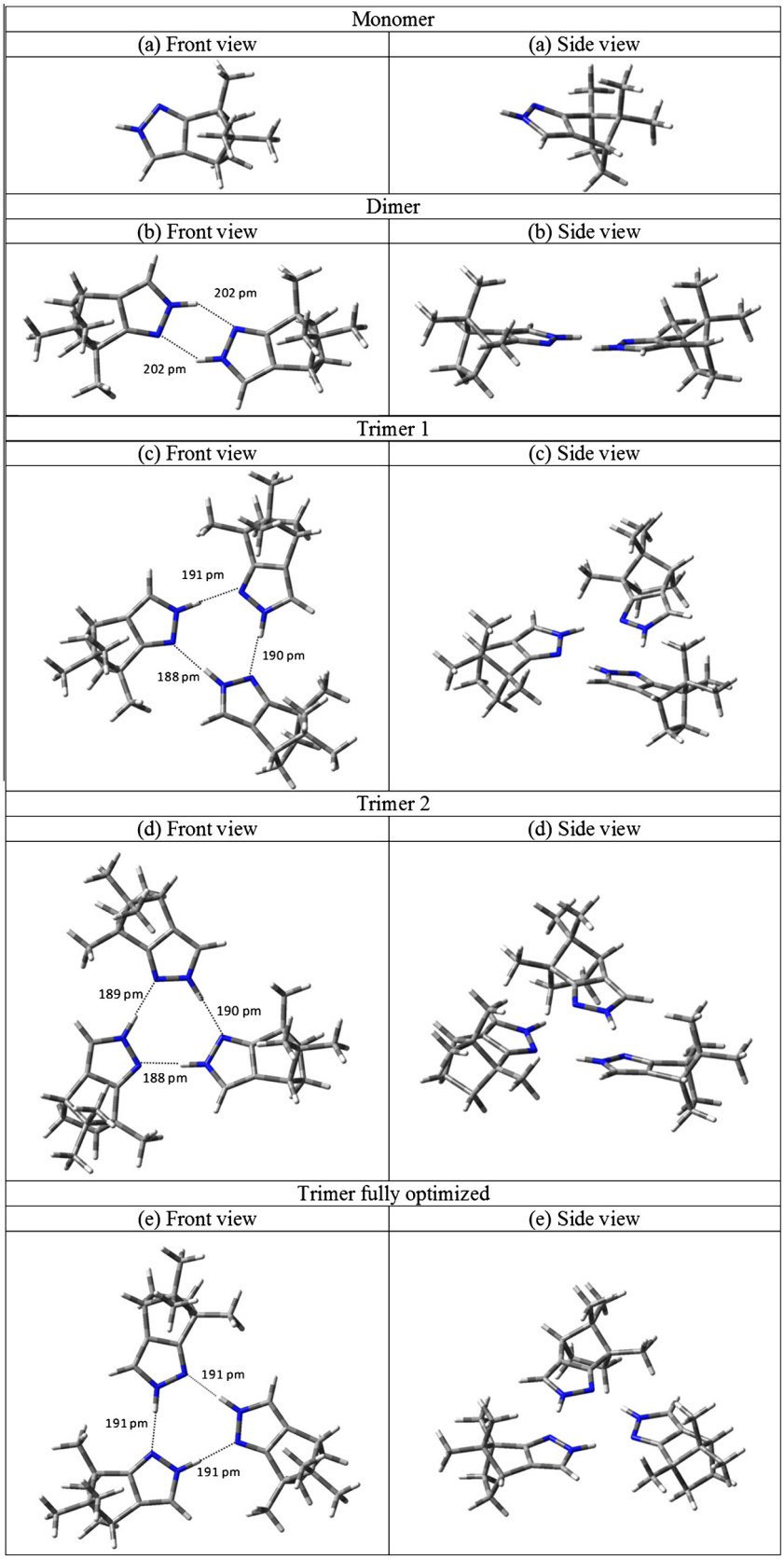

Figure 1. The molecular structure of the monomer (a), the dimer (b), the trimer one (c) the trimer two (d) and the trimer fully optimised (e) of campho[2,3-*c*]pyrazole, showing the N—H···N hydrogen bonds in the case of drimer and trimers.

It is relevant that the thin film and suspension IR spectra (solid phase of the sample) deal with the presence of the trimer structure, and no band can be assigned to the presence of monomers. The CCl_4 solution IR spectra deal with the presence of both monomers

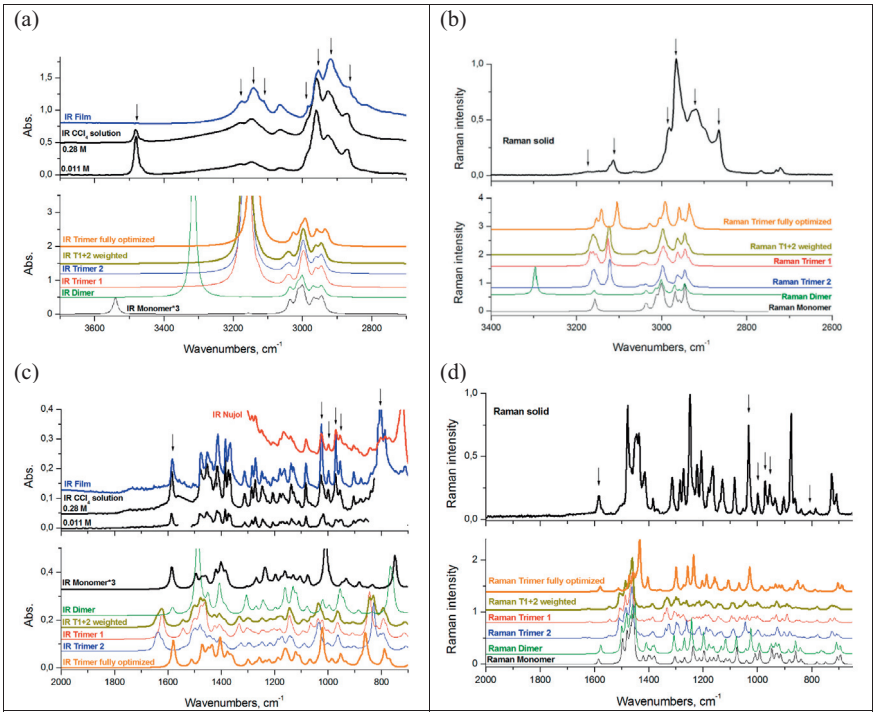

Figure 2. Experimental and scaled predicted IR (panels a and c) and Raman (panels b and d) spectra of **LABHEB** in the 3700–2600 cm^{-1} and in the 2000–700 cm^{-1} spectral regions: (a) experimental IR spectrum in film conditions (top, in blue) and in CCl_4, 0.28 and 0.011 M solutions (top, in black). (b) and (d) experimental Raman spectrum of the solid (top). (c) Experimental IR spectrum in nujol mull (top, in red), in film conditions (top, in blue) and in CCl_4, 0.28 and 0.011 M solutions (top, in black). In all cases, bottom panels show the scaled predicted IR (panels a and c) and Raman (panels b and d) spectra at the B3LYP/6-31G(d) level of theory, for the **LABHEB** monomer (in black), for the dimer (green), for the trimer 1 (in red), for the trimer 2 (in blue), for the contribution of both trimers (brown) and for the trimer fully optimized (orange); NIST scaling frequency factor of 0.96, Lorentzian function, pitch = 1 cm^{-1}, FWHM (Full Width Half Maximum) = 8 cm^{-1}. All of the Raman experimental and theoretical data are normalized. For visibility, the IR spectrum of the monomer is multiplied by 3.

and trimers. The most diluted CCl_4 solution (0.011 M) was mainly formed by monomeric structures, as expected.

Analysis of the spectral zone from 2000 to 700 cm^{-1} gave us additional information (see Figs. 2c and d, 3c and d). The monomer and the trimer seem to be present in the IR spectrum in CCl_4 solution, but the presence of the trimers seems to be enough to reproduce the film and nujol mull IR spectra and the solid Raman spectrum. The band observed at 1585 cm^{-1} (IR, 1583 cm^{-1} in Raman) was assigned to the C═N and C═C bond stretchings of the pyrazole ring. In addition, the experimental band observed at 1024 cm^{-1} (IR, 1026 cm^{-1} in Raman) was assigned to the N—N stretching and vinyl hydrogen wagging of the pyrazole ring.

The experimental bands at 998 cm^{-1} (IR and Raman), 972 cm^{-1} (IR and Raman), and 956 cm^{-1} (IR and Raman) were assigned to the CH_2 rocking and twisting normal modes. The experimental band at 804 cm^{-1} (IR, 807 cm^{-1} in Raman) was assigned to the vinyl hydrogen and N—H waggings of the pyrazole ring.

The solution spectra showed a major proportion of the monomer, especially for the most diluted solutions, but evidence of possible oligomeric structures was found for the most concentrated solutions.

The low frequency region, below 700 cm^{-1}, presented normal modes with contributions of waggings, rockings, and torsions (see Figs. 4 and 5). An example of this is the experimental band observed at 590 cm^{-1} (IR, 591 cm^{-1} in Raman), which corresponds to the N—H and C—H waggings of the campho[2,3-*c*]pyrazole moiety. Other examples are the bands observed at 571 cm^{-1} (IR and Raman) and at 299 cm^{-1} (IR and Raman), which were assigned to the ring deformation. This last band is due to the presence of the trimers. Other examples could be the experimental bands observed at 240 cm^{-1} (IR and Raman) and at 221 cm^{-1} (IR, 220 cm^{-1} in Raman), which were assigned to the CH_3 torsions and ring deformation.

Finally, due to the fact that the monomer does not present any bands below 175 cm^{-1}, the three bands present in the Far-IR and Raman spectra of the solid **LABHEB** at 140 cm^{-1} (IR, 135 cm^{-1} in Raman), 123 cm^{-1} (IR, 128 cm^{-1} in Raman), and at 84 cm^{-1} (IR and Raman) can be assigned to the more complex molecular species, for example, the trimers. The theoretical Far-IR, and Raman spectra calculated for the trimer configurations of **LABHEB** allowed the assignment of the first and second bands (140 and 123 cm^{-1}) to the methyl torsions of the three monomer subunits and the third one (84 cm^{-1}) to the torsion normal modes of one **LABHEB** subunit with respect to the other two subunits and a butterfly motion.

If we compare the B97D and B3LYP theoretical spectra with the experimental ones, we can conclude that the two levels of theory reproduce in a suitable way the experimental spectra. In addition, the theoretical spectra of the trimers both partially and fully optimized are very similar, although there are few bands better predicted by the trimers when fully optimized. An example of this could be the experimental bands at 875 and at 725 cm^{-1} in the Raman spectrum of the solid (see Fig. 2d).

2.3. Chiroptical response

Later we examined the chiroptical properties of **LABHEB** in relation to their structures in different phases by means of the combined use of vibrational circular dichroism (VCD) and computational calculations. In this way, the signs of the rotatory strength would be helpful in determining the chiral self-assembly of **LABHEB** crystals.

We observed a fair agreement between the experimental (in CCl_4 solution and in fluorolube/nujol mulls) and the predicted scaled VCD spectra for the monomer and the trimers of **LABHEB** calculated at the B3LYP/6-31G(d) (Figs. 6 and 8) and B97D/6-31+G(d,p) (Figs. 7 and 9) levels of theory. Figures 6 and 7 display

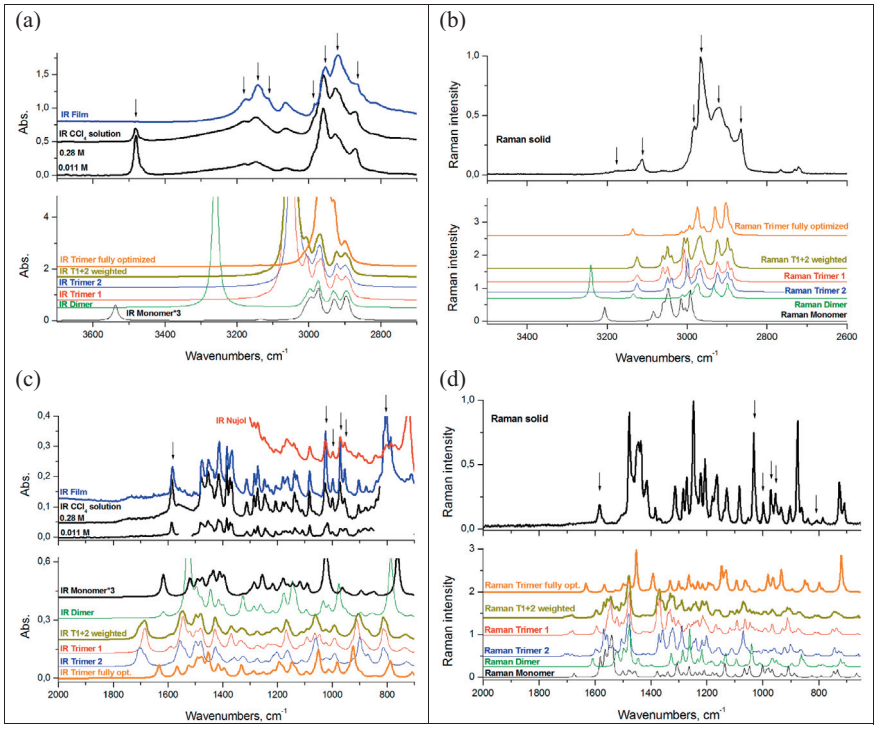

Figure 3. Experimental and scaled predicted IR (panels a and c) and Raman (panels b and d) spectra of **LABHEB** in the 3700–2600 cm^{-1} and in the 2000–700 cm^{-1} spectral regions: (a) experimental IR spectrum in film conditions (top, in blue) and in CCl_4, 0.28 and 0.011 M solutions (top, in black). (b) and (d) experimental Raman spectrum of the solid (top). (c) Experimental IR spectrum in nujol mull (top, in red), in film conditions (top, in blue) and in CCl_4, 0.28 and 0.011 M solutions (top, in black). In all cases, bottom panels show the scaled predicted IR (panels a and c) and Raman (panels b and d) spectra at the B97D/6-31+G(d,p) level of theory, for the **LABHEB** monomer (in black), for the dimer (green), for the trimer 1 (in red), for the trimer 2 (in blue), for the contribution of both trimers (brown) and for the trimer fully optimized (orange); NIST scaling frequency factor of 1.020, Lorentzian function, pitch = 1 cm^{-1}, FWHM (Full Width Half Maximum) = 8 cm^{-1}. All of the Raman experimental and theoretical data are normalized. For visibility, the IR spectrum of the monomer is multiplied by 3.

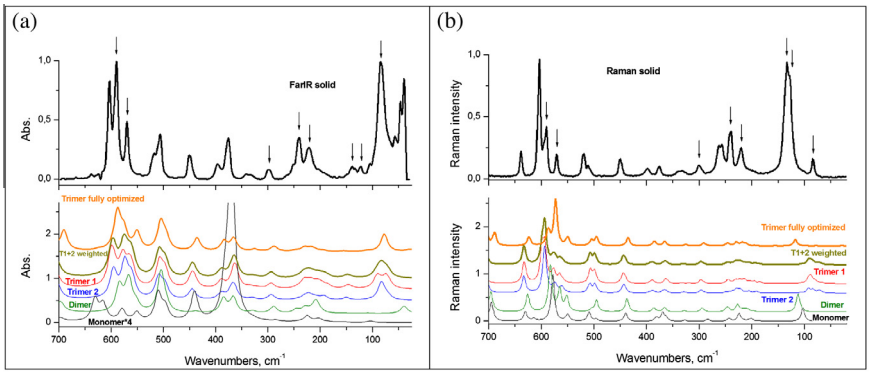

Figure 4. Experimental and scaled predicted Far-IR (panel a) and Raman (panel b) spectra of **LABHEB** in the 700–25 cm^{-1} spectral region: (top) experimental Far-IR spectrum (a) and experimental Raman spectrum (b) of the solid. In both cases, the bottom panels show the scaled predicted IR (panel a) and Raman (panel b) spectra at the B3LYP/6-31G(d) level of theory, for the **LABHEB** monomer (in black), for the dimer (green), for the trimer 1 (in red), for the trimer 2 (in blue), for the contribution of both trimers (brown) and for the trimer fully optimized (orange); NIST scaling frequency factor of 0.96, Lorentzian function, pitch = 1 cm^{-1}, FWHM (Full Width Half Maximum) = 8 cm^{-1}. All of the IR and Raman experimental and theoretical data are normalized. For visibility, the IR spectrum of the monomer is multiplied by 4.

the experimental (in CCl_4 solution) and theoretical VCD spectra of **LABHEB** in the 2000–900 cm^{-1} spectral region and Figures 8 and 9 display the experimental (in fluorolube/nujol mulls) and theoretical VCD spectra of **LABHEB** in the same spectral region. In Figures 6–9, the bottom panels show the predicted scaled VCD spectra for the **LABHEB** monomer (in black), dimer (in green), trimer 1 (in blue), trimer 2 (in red), and trimer fully optimized (orange). The DFT calculations were made in the harmonic approximation. A few experimental VCD bands showed the presence of the monomer or the trimer structures, depending on the phase, that is, the trimers in the solid phase and the monomer in CCl_4 solution.

First, we will comment on the most relevant features of VCD spectra in 0.28 M CCl_4 solution. The five (+, +, +, +, +) bands at 1480, 1448, 1411, 1311, and 1283 cm^{-1} and the two (−, −) bands at 1175 and 1081 cm^{-1} were well predicted by the monomer of the (4*S*,7*R*)-campho[2,3-*c*]pyrazole. However, these bands were not so well reproduced by the theoretical spectra of the trimers. In fact, the last two (−, −) bands at 1175 and 1081 cm^{-1} had the opposite sign (+, +) in the theoretical spectra of the trimers.

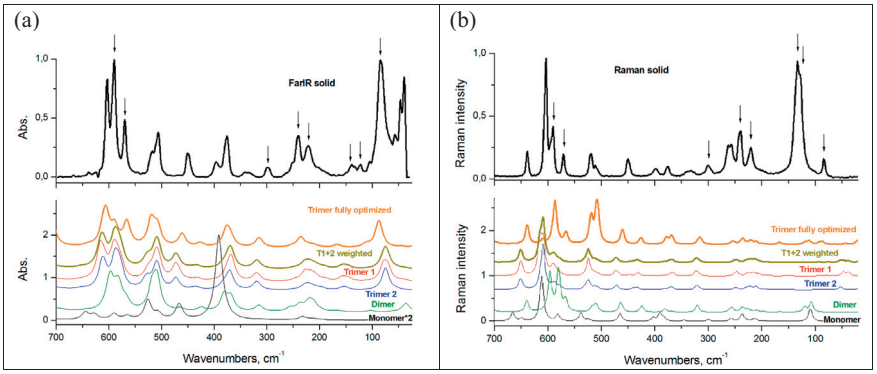

Figure 5. Experimental and scaled predicted Far-IR (panel a) and Raman (panel b) spectra of **LABHEB** in the 700–25 cm^{-1} spectral region: (top) experimental Far-IR spectrum (a) and experimental Raman spectrum (b) of the solid. In both cases, the bottom panels show the scaled predicted IR (panel a) and Raman (panel b) spectra at the B97D/6-31+G(d,p) level of theory, for the **LABHEB** monomer (in black), for the dimer (green), for the trimer 1 (in red), for the trimer 2 (in blue), for the contribution of both trimers (brown) and for the trimer fully optimized (orange); NIST scaling frequency factor of 1.020, Lorentzian function, pitch = 1 cm^{-1}, FWHM (Full Width Half Maximum) = 8 cm^{-1}. All of the IR and Raman experimental and theoretical data are normalized. For visibility, the IR spectrum of the monomer is multiplied by 2.

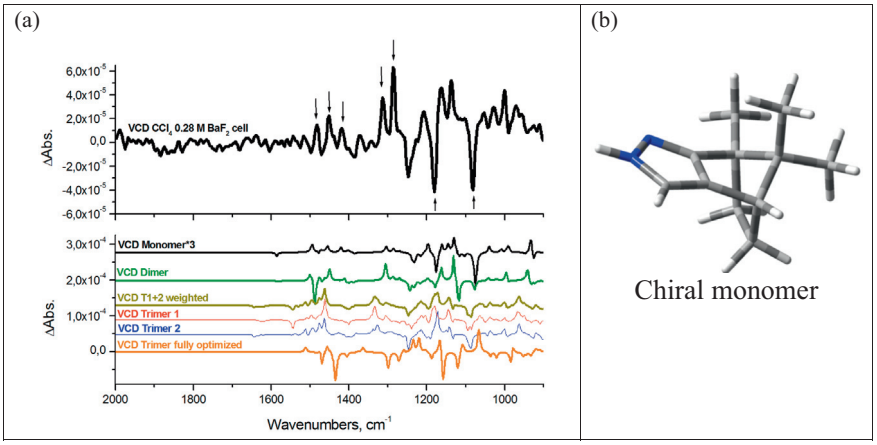

Figure 6. (a) Experimental and theoretical VCD spectra of **LABHEB** in the 2000–900 cm^{-1} spectral region. At the top, the experimental VCD spectrum in CCl_4 (0.28 M solution), with BaF_2 cell (in black), 4000 scans, 4 cm^{-1} of resolution. At the bottom, the predicted scaled VCD spectra at the B3LYP/6-31G(d) level of theory, for the **LABHEB** monomer (in black), for the dimer (green), for the trimer 1 (in red), for the trimer 2 (in blue), for the contribution of both trimers (brown) and for the trimer fully optimized (orange); NIST scaling frequency factor of 0.96, Lorentzian function, pitch = 1 cm^{-1}, FWHM (Full Width Half Maximum) = 8 cm^{-1}. (b) Chiral monomer structure. For visibility, the VCD spectrum of the monomer is multiplied by 3.

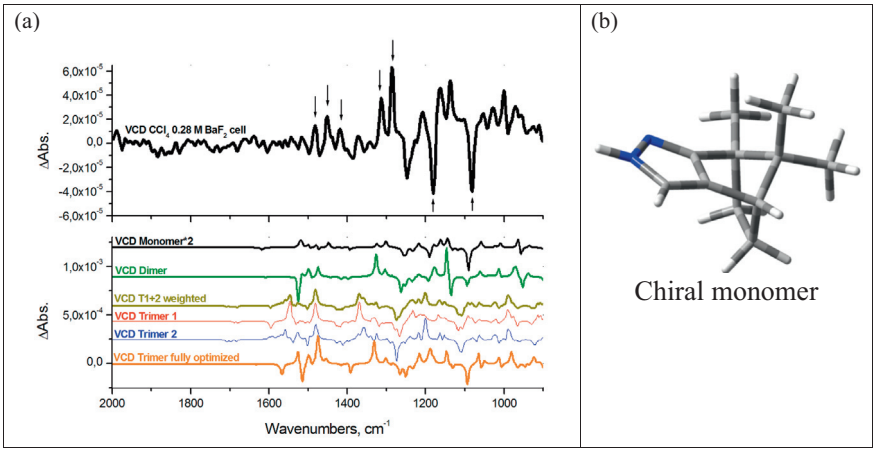

Figure 7. (a) Experimental and theoretical VCD spectra of **LABHEB** in the 2000–900 cm^{-1} spectral region. At the top, the experimental VCD spectrum in CCl_4 (0.28 M solution), with BaF_2 cell (in black), 4000 scans, 4 cm^{-1} of resolution. At the bottom, the predicted scaled VCD spectra at the B97D/6-31+G(d,p) level of theory, for the **LABHEB** monomer (in black), for the dimer (green), for the trimer 1 (in red), for the trimer 2 (in blue), for the contribution of both trimers (brown) and for the trimer fully optimized (orange); NIST scaling frequency factor of 1.020, Lorentzian function, pitch = 1 cm^{-1}, FWHM (Full Width Half Maximum) = 8 cm^{-1}. (b) Chiral monomer structure. For visibility, the VCD spectrum of the monomer is multiplied by 2.

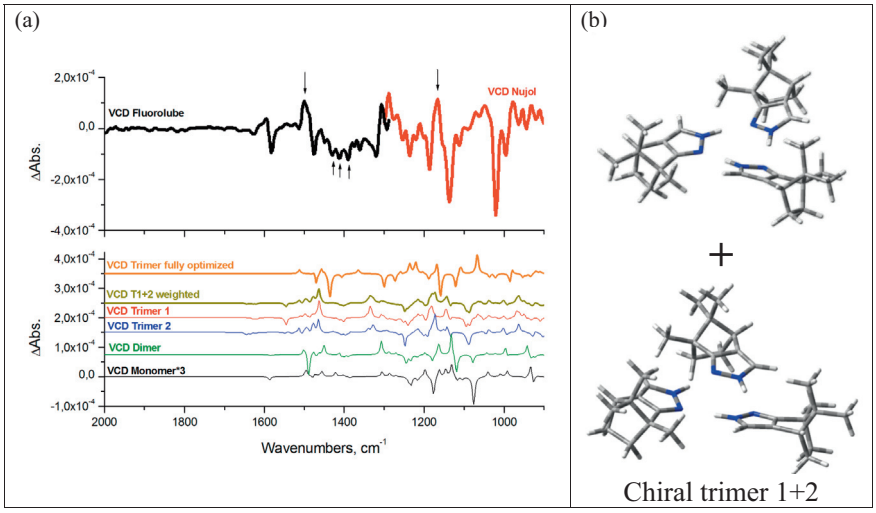

Figure 8. (a) Experimental and theoretical VCD spectra of **LABHEB** in the 2000–900 cm^{-1} spectral region. At the top, the experimental VCD spectrum in fluorolube mull (in black) and in nujol mull (in red), 8000 scans, 4 cm^{-1} of resolution. At the bottom, the predicted scaled VCD spectra at the B3LYP/6-31G(d) level of theory, for the **LABHEB** monomer (in black), for the dimer (green), for the trimer 1 (in red), for the trimer 2 (in blue), for the contribution of both trimers (brown) and for the trimer fully optimized (orange); NIST scaling frequency factor of 0.96, Lorentzian function, pitch = 1 cm^{-1}, FWHM (Full Width Half Maximum) = 8 cm^{-1}. (b) Chiral trimer structure. For visibility, the VCD spectrum of the monomer is multiplied by 3.

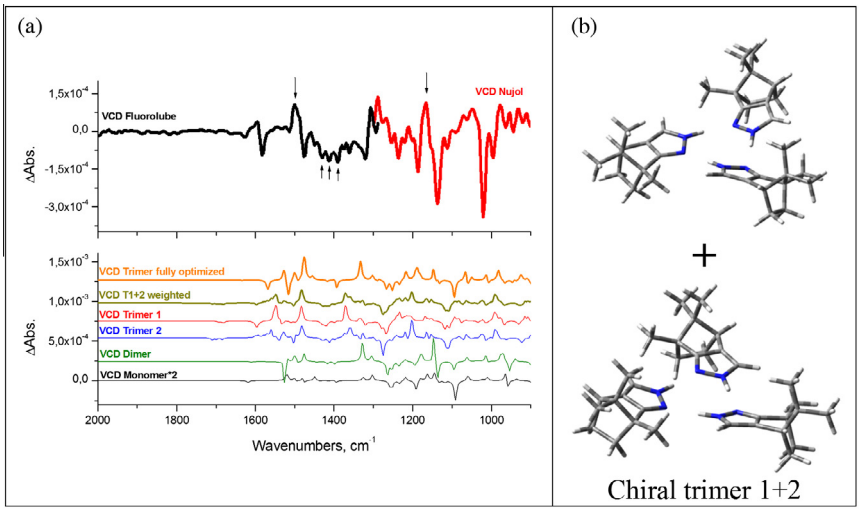

Figure 9. (a) Experimental and theoretical VCD spectra of **LABHEB** in the 2000–900 cm^{-1} spectral region. At the top, the experimental VCD spectrum in fluorolube mull (in black) and in nujol mull (in red), 8000 scans, 4 cm^{-1} of resolution. At the bottom, the predicted scaled VCD spectra at the B97D/6-31+G(d,p) level of theory, for the **LABHEB** monomer (in black), for the dimer (green), for the trimer 1 (in red), for the trimer 2 (in blue), for the contribution of both trimers (brown) and for the trimer fully optimized (orange); NIST scaling frequency factor of 1.020, Lorentzian function, pitch = 1 cm^{-1}, FWHM (Full Width Half Maximum) = 8 cm^{-1}. (b) Chiral trimer structure. For visibility, the VCD spectrum of the monomer is multiplied by 2.

The band observed at 1480 cm^{-1} (VCD, 1479 cm^{-1} in IR and Raman) was assigned to the CH_2 rocking and asymmetric CH_3 bending. The experimental band at 1448 cm^{-1} (VCD, 1445 cm^{-1} in IR and Raman) was assigned to the framework deformation. Another noteworthy band was observed at 1411 cm^{-1} (VCD, IR and Raman) and was assigned to the N—H wagging and C=N stretching. The experimental bands observed at 1311 cm^{-1} (VCD, 1309 cm^{-1} in IR and Raman) and at 1283 cm^{-1} (VCD, IR and Raman) were assigned to the CH_2 and C—H waggings. Finally, the experimental bands at 1175 cm^{-1} (VCD, 1172 cm^{-1} in IR and Raman) and at 1081 cm^{-1} (VCD, IR, and Raman) were assigned to the framework deformation normal mode. The VCD signals of the 0.011 M solution were too weak to be analyzed.

Second, the VCD spectra in fluorolube and those of the nujol mulls were in better agreement with the predicted VCD spectra of the trimers than those of the monomer. One example is the (+) band observed at 1497 cm^{-1} (VCD, 1479 cm^{-1} in IR and Raman), which was assigned to the CH_2 rocking and asymmetric CH_3 bending normal mode. Other noteworthy (–, –, –) bands were observed at 1427 cm^{-1} (VCD, 1435 cm^{-1} in IR and 1430 cm^{-1} in Raman), 1411 cm^{-1} (VCD, IR and Raman), and at 1385 cm^{-1} (VCD, 1384 cm^{-1} in IR and Raman) and were assigned to the symmetric CH_3 bending. A last example is the (+) band observed at 1165 cm^{-1} (VCD, IR, and Raman), which was assigned to the framework deformation.

The literature contains examples about how the assignments were made in similar situations[18,19] especially in the case of bonds involved in H-bonding.[20]

In conclusion, the monomer model predicts better the experimental VCD spectrum in CCl_4 solution than the dimer or trimers, although oligomeric structures may be present too, especially for the most concentrated solutions.[21] On the other hand,

the experimental VCD spectra in fluorolube/nujol mulls are better predicted by the trimers models, which are present in the solid phase.[4,15]

3. Conclusion

We have measured the IR (including FarIR), VCD, and Raman spectra of (4*S*,7*R*)-campho[2,3-*c*]pyrazole in solution as well as in the solid-state, and we have assigned all of the bands, excluding overtones and combinations, based on scaled B3LYP/6-31G(d) and B97D/6-31+G(d,p) calculations. We have proved that the comparison of VCD spectra in CCl_4 solution and in nujol/fluorolube mulls with those calculated for the chiral monomer, dimer, and trimers, allows us to determine the self-assembly of **LABHEB** crystals. Trimers are the only ones present in the crystal. Our results are in agreement with the absolute configuration previously determined for this species from crystallographic and solid CPMAS NMR studies.[10] The solution spectra show a major proportion of monomers, especially for the most dilute solutions, but evidence of possible oligomeric structures has been found for the more concentrated solutions. The analysis of the low frequency region (700–25 cm^{-1}) in the FT-Raman and Far-IR spectra provides important information in order to determine the presence of trimers in the solid phase. Regarding the theoretical methods, the results obtained at the B3LYP/6-31G(d) and B97D/6-31+G(d,p) levels are comparable and any of them could be used. With regard to the optimization of hydrogen-bonded structures (in our case **LABHEB** trimers), the results are very similar but the fully optimized geometry appears to be slightly better. Contrary to ^{13}C solid-state NMR predictions, where fully optimized geometries are totally inadequate, for vibrational spectra, full optimization should be preferred, unless both spectroscopies are compared.

4. Experimental

4.1. Sample preparation

Good quality crystals of **LABHEB** were obtained from a solution of the pure compound[10] in dichloromethane at room temperature, to which hexane was added until turbidity appears.

4.2. Vibrational spectroscopy (Far-IR, IR, and Raman)

The Far-IR spectrum of **LABHEB** in the solid phase was recorded using a Bruker Vertex 70 in the 700–25 cm^{-1} region, with a resolution of 4 cm^{-1} and 200 scans, and the platinum ATR accessory (single reflection diamond ATR accessory) and the silicon beamsplitter for the Far-IR region.

A FT-IR 4100 JASCO spectrometer, equipped with a Globar source, a DGTS detector, and KBr optics, was used to record the IR spectrum of 0.28 M and 0.011 M solutions (in CCl_4) using a standard liquid cell equipped with KBr windows. For the film spectrum we prepared a very low concentration solution in CCl_4 of the sample and we evaporated the solvent under anhydrous conditions in order to obtain a very thin film of the sample, which was measured. Finally, we recorded the ATR spectrum for the solid sample. The IR spectrum was recorded in the 4000–400 cm^{-1} range with a resolution of 1 cm^{-1} and 200 scans.

The Raman spectrum of **LABHEB** was recorded using a MultiRAM Stand Alone FT-Raman Spectrometer, equipped with an Nd:YAG laser (excitation line at 1064 nm) and a Ge detector cooled at liquid nitrogen temperature. The spectrum was measured using a standard solid support with a resolution of 1 cm^{-1} and 200 scans.

4.3. VCD

The VCD spectra of **LABHEB** in the fluorolube and nujol mulls were recorded using a JASCO FVS-4000 FTIR spectrometer, equipped with MCTV (2000–800 cm^{-1}) detector. A few milligrams of **LABHEB** were mixed with fluorolube or nujol mineral oils in order to obtain suitable mulls. Special attention is needed when working with solid samples in circular dichroism spectroscopy.[22–24] We measured the mulls in several positions by rotating the sample around both the beam propagation axes (90° and 180°) and that perpendicular to it (180°) in order to obtain the true VCD peaks in order to minimize the presence of artifacts.[22] All spectra were recorded using a standard cell equipped with BaF_2 windows, with a resolution of 4–8 cm^{-1}, path lengths between 6–50 microns and 4000–8000 scans by blocks of 2000 scans. Finally, the 0.28 M solution (in CCl_4) was also recorded. Concerning the baseline correction, we have subtracted the nujol and/or fluorolube signals for the suspension spectra and the solvent signal for the solution spectrum.

4.4. Computational details

Calculations have been carried out at the widespread B3LYP/6-31G(d)[25,26] and the recent long-range dispersion-corrected Grimme's functional (B97D),[27] which was demonstrated to provide realistic binding energies and intermolecular distances, and the 6-31+G(d,p) basis set using the facilities of the Gaussian 09 package.[28] The geometry of the monomer, the dimer, and the trimers was fully optimized (no imaginary frequencies). In the case of the trimer, the position of the non-hydrogen atoms was also fixed at the positions determined by X-ray crystallography and hydrogen atoms have been optimized. The harmonic vibrations have been scaled using a single factor, 0.960 and 1.020, from the NIST database[17] for the B3LYP/6-31G(d) and B97D/6-31+G(d,p) levels, respectively. All of the calculated IR-VCD spectra were simulated with 100 μm of cell path length and concentration 1 M.

Acknowledgements

This work was supported by the Junta de Andalucía (project P08-FQM-04096). The authors thank the University of Jaén for continuing financial support and its CICT for instrumental facilities. MMQM thanks the university of Jaén for a postdoctoral fellowship. Authors also thank the Ministerio de Ciencia e Innovación (Project Nos. CTQ2012-35513-C02-02, CTQ2010-16122, CTQ2009-12520-C03-3 and CONSOLIDER CSD2007-00041), the Comunidad Autónoma de Madrid (Project MADRISOLAR2, Ref. S2009/PPQ-1533), for continuing support. Thanks are also given to the CTI (CSIC) for the allocation of computer time.

References

1. (a) De Paz, J. L. G.; Elguero, J.; Foces-Foces, C.; Llamas-Saíz, A. L.; Aguilar-Parrilla, F.; Klein, O.; Aguilar- Parrilla, H. H. *J. Chem. Soc., Perkin Trans. 2* **1997**, 101–109; (b) Foces-Foces, C.; Alkorta, I.; Elguero, J. *Acta Crystallogr., Sect. B* **2000**, *56*, 1018–1028; (c) Alkorta, I.; Elguero, J.; Foces-Foces, C.; Infantes, L. *Arkivoc* **2006**, *ii*, 15–30.
2. (a) Foces-Foces, C.; Hager, O.; Jagerovic, N.; Jimeno, M. L.; Elguero, J. *Chem. Eur. J.* **1997**, *3*, 121–126; (b) García, M. A.; López, C.; Claramunt, R. M.; Kenz, A.; Pierrot, M.; Elguero, J. *Helv. Chim. Acta* **2002**, *85*, 2763–2776.
3. (a) Baldy, A.; Elguero, J.; Faure, R.; Pierrot, M.; Vincent, E. J. *J. Am. Chem. Soc.* **1985**, *107*, 5290–5291; (b) Smith, J. A. S.; Wehrle, B.; Aguilar-Parrilla, F.; Limbach, H.-H.; Foces, M. C.; Cano, F. H.; Elguero, J.; Baldy, A.; Pierrot, M.; Khurshid, M. M. T.; Larcombe, J. B. *J. Am. Chem. Soc.* **1989**, *111*, 7304–7312; (c) Aguilar-Parrilla, F.; Scherer, G.; Limbach, H.-H.; Foces-Foces, C.; Cano, F. H.; Elguero, J. *J. Am. Chem. Soc.* **1992**, *114*, 9657–9659; (d) Foces-Foces, C.; Echevarría, A.; Jagerovic, N.; Alkorta, I.; Elguero, J.; Langer, U.; Klein, O.; Minguet-Bonvehí, M.; Limbach, H.-H. *J. Am. Chem. Soc.* **2001**, *123*, 7898–7906; (e) Klein, O.; Aguilar-Parrilla, F.; López, J. M.; Jagerovic, N.; Elguero, J.; Limbach, H.-H. *J. Am. Chem. Soc.* **2004**, *126*, 11718–11732.

4. Llamas-Saiz, A.; Foces-Foces, C.; Sobrados, I.; Elguero, J.; Meutermans, W. *Acta Crystallogr., Sect. C* **1993**, *49*, 724–729.
5. Foces-Foces, C.; Cano, F. H.; Elguero, J. *Gazz. Chim. Ital.* **1993**, *123*, 477–479.
6. Moreno-Mañas, M.; Sebastián, R. M.; Vallribera, A.; Piniella, J. F.; Alvarez-Larena, A.; Jimeno, M. L.; Elguero, J. *New J. Chem.* **2001**, *25*, 329–335.
7. Faure, R.; Frideling, A.; Galy, J.-P.; Alkorta, I.; Elguero, J. *Heterocycles* **2002**, *57*, 307–316.
8. Frideling, A.; Faure, R.; Galy, J.-P.; Kenz, A.; Alkorta, I.; Elguero, J. *Eur. J. Med. Chem.* **2004**, *39*, 37–48.
9. (a) Teichert, J.; Oulié, P.; Jacob, K.; Vendier, L.; Etienne, M.; Claramunt, R. M.; López, C.; Pérez Medina, C.; Alkorta, I.; Elguero, J. *New J. Chem.* **2007**, *31*, 936–946; (b) Avilés Moreno, J. R.; Quesada Moreno, M. M.; López González, J. J.; Claramunt, R. M.; López, C.; Alkora, I.; Elguero, J. *ChemPhysChem* **2013**, *14*, 3355–3360.
10. (a) Webber, A. L.; Emsley, L.; Claramunt, R. M.; Brown, S. P. *J. Phys. Chem. A* **2010**, *114*, 10435–10442; (b) Yap, G. P. A.; Claramunt, R. M.; López, C.; García, M. A.; Pérez-Medina, C.; Alkorta, I.; Elguero, J. *J. Mol. Struct.* **2010**, *965*, 74–81.
11. López González, J. J.; Partal Ureña, F.; Avilés Moreno, J. R.; Mata, I.; Molins, E.; Claramunt, R. M.; Lopez, C.; Alkorta, I.; Elguero, J. *New J. Chem.* **2012**, *36*, 749–758.
12. Alkorta, I.; Elguero, J.; Roussel, C.; Vanthuyne, N.; Piras, P. *Adv. Heterocycl. Chem.* **2012**, *105*, 1–188.
13. Cambridge Structural Database (a) Allen, F. H. *Acta Crystallogr., Sect. B* **2002**, *58*, 380–388; (b) Allen, F. H.; Motherwell, W. D. S. *Acta Crystallogr., Sect. B* **2002**, *58*, 407–422; (c) CSD version 5.32, updated Feb. 2011. http://www.ccdc.cam.ac.uk.
14. Foces-Foces, C. *Acta Crystallogr., Sect. E* **2005**, *61*, o337–o339.
15. LABHEB01, Doro, F.; Bailey, P.; Parsons, S. 2007, Private Communication.
16. (a) Partal Ureña, F.; Avilés Moreno, J. R.; González López, J. J. *J. Phys. Chem. A* **2008**, *112*, 7887–7893; (b) Avilés Moreno JR, J. R.; Partal Ureña, F.; López González, J. J. *Phys. Chem. Chem. Phys.* **2009**, *11*, 2459–2467; (c) Avilés Moreno, J. R.; Quesada Moreno, M. M.; Partal Ureña, F.; Avilés Moreno JR, J. J.; López González, J. J. *Tetrahedron: Asymmetry* **2012**, *23*, 1084–1092; (d) Huet, T. R.; Avilés Moreno, J. R.; Pirali, O.; Tudorie, M.; Partal Ureña, F.; López González, J. J. *Quant. Spectrosc. Radiat. Transfer.* **2012**, *113*, 1261–1265; (e) Partal Ureña, F.; Avilés Moreno, J. R.; López González, J. J. *Chirality* **2010**, *22*, E123–E129; (f) Avilés Moreno, J. R.; López González, J. J.; Partal Ureña, F.; Vera, F.; Ros, M. B.; Sieera, T. *J. Phys. Chem. B* **2012**, *116*, 5090–5096.
17. NIST Standard Reference Database 101; Computational Chemistry Comparison and Benchmark DataBase: http://cccbdb.nist.gov/vibscalejust.asp.
18. Freedmand, T. B.; Cao, X.; Young, D. A.; Nafie, L. A. *J. Phys. Chem. A* **2002**, *106*, 3560–3565.
19. Nicu, V. P.; Autschbach, J.; Baerends, E. J. *Phys. Chem. Chem. Phys.* **2009**, *11*, 1526–1538.
20. Nicu, V. P.; Heshmath, M.; Baerends, E. J. *Phys. Chem. Chem. Phys.* **2011**, *13*, 8811–8825.
21. (a) Tabacik, V.; Pellegrin, V.; Günthard, H. H. *Spectrochim. Acta* **1979**, *35A*, 1055–1081; (b) Orza, J. M.; García, M. V.; Alkorta, I.; Elguero, J. *Spectrochim. Acta, Part A* **2000**, *56*, 1469–1498; (c) Castaneda, J. P.; Denisov, G. S.; Kucherov, S. Y.; Schreiber, V. M.; Shurukhina, A. V. *J. Mol. Struct.* **2003**, *660*, 25–40; (d) Rice, C. A.; Borho, N.; Suhm, M. A. Z. *Phys. Chem.* **2005**, *219*, 379–388; (e) Wassermann, T. N.; Rice, C. A.; Suhm, M. A.; Luckhaus, D. *J. Chem. Phys.* **2007**, *127*. 234309-1-9.
22. (a) Kuroda, R.; Harada, T.; Shindo, Y. *Rev. Sci. Instrum.* **2004**, *72*, 3802–3810; (b) Shindo, Y. *Opt. Eng.* **1995**, *34*, 3369–3384; (c)*Vibrational Optical Activity. Principles and Applications*; Nafie, L. A., Ed.; Wiley, 2011; p 243. Chapter 8.2.5.
23. Merten, C.; Kowalik, T.; Hartwig, A. *Appl. Spectrosc.* **2008**, *62*, 901–905.
24. Buffeteau, T.; Lagugné-Labarthet, F.; Sourisseau, C. *Appl. Spectrosc.* **2005**, *59*, 732–745.
25. (a) Becke, A. D. *Phys. Rev. A: At. Mol. Opt. Phys.* **1988**, *38*, 3098–3100; (b) Becke, A. D. *J. Chem. Phys.* **1993**, *98*, 5648–5652; (c) Lee, C.; Yang, W.; Parr, R. G. *Phys. Rev. B* **1988**, *37*, 785–789.
26. Hariharan, P. A.; Pople, J. A. *Theor. Chim. Acta* **1973**, *28*, 213–222.
27. Grimme, S. *J. Comput. Chem.* **2006**, *27*, 1787–1799.
28. Frisch, M. J.; Trucks, G. W.; Schlegel, H. B.; Scuseria, G. E.; Robb, M. A.; Cheeseman, J. R.; Scalmani, G.; Barone, V.; Mennucci, B.; Petersson, G. A.; Nakatsuji, H.; Caricato, M.; Li, X.; Hratchian, H. P.; Izmaylov, A. F.; Bloino, J.; Zheng, G.; Sonnenberg, J. L.; Hada, M.; Ehara, M.; Toyota, K.; Fukuda, R.; Hasegawa, J.; Ishida, M.; Nakajima, T.; Honda, Y.; Kitao, O.; Nakai, H.; Vreven, T., ; Montgomery, J. A., Jr.; Peralta, J. E.; Ogliaro, F.; Bearpark, M.; Heyd, J. J.; Brothers, E.; Kudin, K. N.; Staroverov, V. N.; Kobayashi, R.; Normand, J.; Raghavachari, K.; Rendell, A.; Burant, J. C.; Iyengar, S. S.; Tomasi, J.; Cossi, M.; Rega, N.; Millam, J. M.; Klene, M.; Knox, J. E.; Cross, J. B.; Bakken, V.; Adamo, C.; Jaramillo, J.; Gomperts, R.; Stratmann, R. E.; Yazyev, O.; Austin, A. J.; Cammi, R.; Pomelli, C.; Ochterski, J. W.; Martin, R. L.; Morokuma, K.; Zakrzewski, V. G.; Voth, G. A.; Salvador, P.; Dannenberg, J. J.; Dapprich, S.; Daniels, A. D.; Farkas, Ö.; Foresman, J. B.; Ortiz, J. V.; Cioslowski, J.; Fox, D. J. *GAUSSIAN09; Revision D.01*; Gaussian: Wallingford, CT, 2009.